Accepted Manuscript

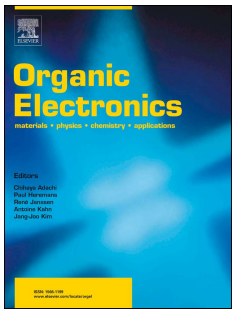

Control of morphological and electrical properties of flexographic printed electronics through tailored ink rheology

Miles L. Morgan, Dan J. Curtis, Davide Deganello

PII: S1566-1199(19)30255-1

DOI: https://doi.org/10.1016/j.orgel.2019.05.027

Reference: ORGELE 5262

To appear in: *Organic Electronics*

Received Date: 15 April 2019

Revised Date: 14 May 2019

Accepted Date: 14 May 2019

Please cite this article as: M.L. Morgan, D.J. Curtis, D. Deganello, Control of morphological and electrical properties of flexographic printed electronics through tailored ink rheology, *Organic Electronics* (2019), doi: https://doi.org/10.1016/j.orgel.2019.05.027.

Control of morphological and electrical properties of flexographic printed electronics through tailored ink rheology

Miles L. Morgan[a], Dan J. Curtis[b], Davide Deganello*[a]

[a]*Welsh Centre for Printing and Coating, College of Engineering, Swansea University, UK*
[b]*Complex Fluids Research Group, College of Engineering, Swansea University, UK*

Abstract

Functional model inks were formulated and printed using flexography in order to assess the influence of ink extensional elasticity and print velocity on the morphological and electrical properties of printed layers. Increased extensional elasticity and higher print velocity resulted in the printing of more isotropic prints, both morphologically and electronically. Furthermore, a correlation between the prints' morphological and electrical anisotropy strongly suggests that print uniformity has a considerable influence on functionality and that ink rheology may be used to control such characteristics.

Keywords: Flexography, rheology, printed electronics, extensional flow, elasticity

1. Introduction

Flexography is a roll-to-roll printing process that is well-established in the packaging industry and capable of high speed, patterned deposition of fluids of a range of viscosities [1]. As such, the technique is considered to have tremendous potential in the mass-production of printed electronic devices. Conductive grids [2], transistors [3], biosensors [4] and photovoltaics [5, 6] all have been fabricated using flexography. Furthermore, this low-waste process can be performed at ambient temperature with flexible substrates. However, unlike the more subjective nature of graphical print applications, prints for electronics purposes have a greater requirement for good print uniformity. Poor uniformity will limit the conductivity of a print leading to functional variation and short circuits in multi-layered devices. Understanding the causes of such non-uniformity is therefore of considerable interest so that they may be controlled and even exploited.

A common cause of non-uniformity in flexographic printing is the phenomenon of "viscous fingering", sometimes referred to as ribbing [7, 8, 9, 10]. Viscous fingering has been attributed to the Saffman-Taylor instability that occurs when a less viscous fluid displaces a more viscous fluid [11]. In the context of flexographic printing it is thought that viscous fingering occurs as the ink is split after the nip between the printing plate and the freshly inked substrate, as illustrated in Figure 1. Their separation creates a dynamic meniscus between air and the ink which is subjected to both shear and extensional stresses [7]. Competition between viscous and surface tension forces typically leads to the formation of fingers with a characteristic wavelength which decreases with the dimensionless capillary number $Ca = \eta v/\sigma$ (where v is printing velocity and η and σ are fluid shear viscosity and surface tension, respectively) [7, 12]. However, this parameter does not consider viscoelastic fluid properties which are often displayed in functional printing inks (that typically contain significant amounts of polymer binder and solid parti-

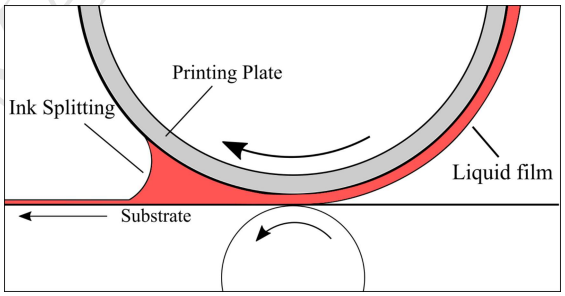

Figure 1: Illustration of ink splitting in flexography as the printing plate and the substrate are separated.

Email address: D.Deganello@swansea.ac.uk (Davide Deganello*)

cles of various shapes and sizes). The Deborah number, defined as the ratio of the material relaxation time λ and the characteristic time scale of the flow T is often used to characterise viscoelasticity in complex flows [13]. In the present context, T may be described in terms of v and ink thickness at the nip l [14, 15]:

$$De = \frac{\lambda}{T} = \frac{\lambda v}{l} \tag{1}$$

While work has been done concerning instabilities including ribbing and filamentation in other roller processes such as forward roll coating [16, 17, 18], little has focussed on their occurrence in flexography. Some analysis has been carried out with respect to the wavelength of the features across the print [8, 12] but this does not consider how such features evolve in the printing direction. This may be of particular interest as ribs in forward roll coating become unsteady as Ca is increased resulting in oscillation, wandering and merging while evolving into septa downstream [19, 20]. Recently it was reported that features induced by instabilities in flexography became significantly smaller with increased ink elasticity. This effect can be linked to filamentation [21] - a phenomenon characteristic of the extensional flows that are often observed in roller processes [17, 22]. Resultant prints can therefore exhibit various morphologies including continuous stripes, branching and dotting [21]. Direct relation of such morphological phenomena to electrical performance has not been carried out, although feature size and orientation is likely to have a considerable effect in this regard.

Herein, a set of printable, conductive fluids were formulated that display identical rheological properties under shear but with markedly different behaviour in extensional flow. As such, the influence of ink extensional properties and printing velocity on the uniformity and subsequent functionality of prints was isolated and examined.

2. Experimental

2.1. Ink formulation

Model inks were formulated by modifying the printable elastic fluids of Morgan et al. [21] with the addition of a poly(3,4-ethylenedioxythiophene) polystyrene sulfonate (PEDOT:PSS) solution to provide electrical conductivity. Solutions of polyvinyl alcohol (PVA) of molecular weight 20-30 x 10^3 g/mol and degree of hydrolysis 88% (Acros Organics) in deionised water were mixed with a water-based Orgacon PEDOT:PSS solution by Agfa (modified S305 with 1.7 wt% PEDOT:PSS) before the addition of aqueous E122 azorubine dye (FastColors LLP) to highlight printed patterns and polyacrylamide (PAM) of molecular weight 5-6 x 10^6 g/mol (Acros Organics) in deionised water to provide extensional elasticity. The respective compatibility of PVA and PAM with PEDOT:PSS is well-documented [23, 24, 25] and the present formulations combine the properties of each in a flexographically printable set of fluids. The contents of the three inks formulated are shown in Table 1. When dried, a solid film of each ink therefore contained 38.7wt% PEDOT:PSS.

Table 1: Solid weight contents of formulated inks.

Ink	PEDOT:PSS (wt%)	PVA (wt%)	PAM (wt%)	Dye (wt%)
P0	1.09	1.625	0	0.1
P1	1.09	1.6125	0.0125	0.1
P2	1.09	1.6	0.025	0.1

2.2. Ink characterisation

Apparent shear viscosity was measured using a Malvern Bohlin Gemini HR Nano rheometer with a 40 mm, 4° stainless steel cone and plate geometry between shear rates of 0.1 and 100 s^{-1}. Small amplitude oscillatory shear (SAOS) measurements were performed using a TA Instruments AR-G2 rheometer with a 60 mm aluminium parallel plate geometry and a gap of 350 µm. Frequency sweeps were carried out at a constant stress of 0.2 Pa which was within the linear viscoelastic region of all inks. All measurements were performed at 20 °C. Due to the extensional flows present in roller processes, a custom built capillary breakup extensional rheometer (CaBER) was used to characterise the uniaxial extensional properties of the inks. CaBER has been utilised for the characterisation of fluids in a range of applications including roller processing [26], drag reduction [27] and electrospinning [28]. In this method a small volume of fluid is loaded between two plates that are then separated in a step strain causing a liquid filament to form and subsequently break under capillary, viscous and/or elastic stresses. [29] By monitoring the evolution of the capillary midfilament diameter $D_{mid}(t)$ with time this technique enables the calculation of extensional viscosity as

$$\eta_E = (2X - 1)\frac{\sigma}{-dD_{mid}/dt} \tag{2}$$

where σ is the ink surface tension and X is a dimensionless variable dependent on the tensile force and radius of

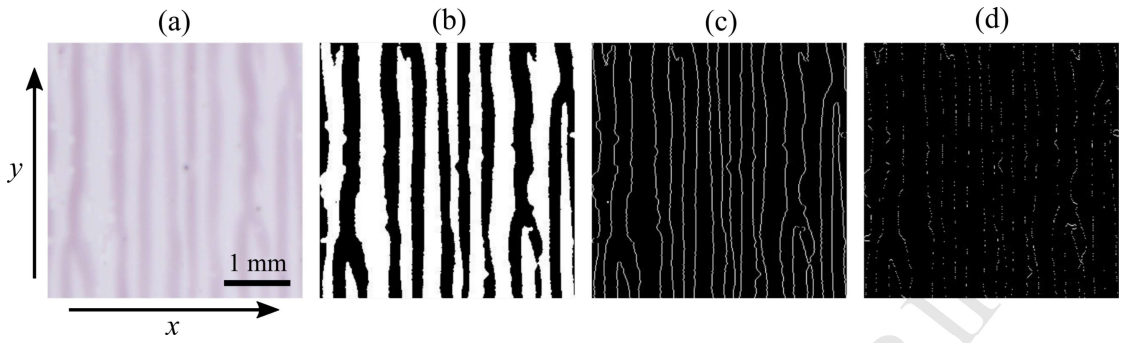

Figure 2: (a) A print area that has been (b) binarised and subjected to feature analysis in the (c) x- and (d) y-direction.

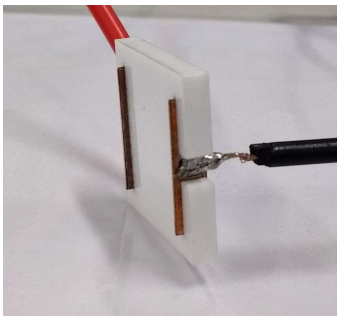

Figure 3: Directional resistance probe.

the filament [30]. X is taken to be 0.7127 for Newtonian fluid breakup [31] while for elastic breakup $X = 1$ due to the axial symmetry of the filament [32]. Idealised elastic filament breakup may be modelled as

$$\frac{D_{mid}(t)}{D_1} = \exp(-t/3\lambda_E) \tag{3}$$

where D_1 is mid-filament diameter just after extension, t is time and λ_E is the fluid's characteristic relaxation time for the elastocapillary thinning action [33]. A plate diameter of 3 mm was used for the CaBER experiments and filament breakup was filmed using a FastCam Mini high speed camera at frame rates between 1000 and 4000 frames per second.

Ink density was determined with a pycnometer and surface tension using a pendant drop method [34] with images taken using the FastCam camera and analysed with ImageJ software. [35]

2.3. Flexographic printing and uniformity analysis

Inks were printed on 250 µm polyethylene terephthalate (PET) with an IGT F1 Printability Tester. Printing and anilox forces of 50 N were used with print velocities of 0.2, 0.6 and 1.0 m/s and a 24 cm^3/m^2 anilox. Solid area, 100% nominal coverage printing plates consisting of a 3 cm wide strip were selected to assist in the analysis of print uniformity. After drying at room temperature, the prints were cut to 20x20 mm squares and digitised with an Epson Perfection V700 scanner at 2000 dots per inch. Areas of each scan 1260x1260 pixels in size (16x16 mm) were used for morphological analysis which was performed using Wolfram Mathematica [36] as follows.

A two dimensional approach was employed in the characterisation of print uniformity which is illustrated in Figure 2. Digitised images were binarised with the threshold determined using Otsu's method [37] before being subjected to a median filter with a radius of 1 pixel (12.7 µm) to suppress the influence of noise whilst retaining the features of interest. Transitions from black to white pixels were counted along each row (x-direction) and down each column (y-direction) before their respective means were calculated. These quantities, once scaled according to the image resolution, therefore represent twice the average wavenumber k of the ink features in each direction. Hence, the wavenumbers k_x and k_y describe the general spatial frequency of the undulations on the print perpendicular and parallel to the printing direction respectively. The ratio k_y/k_x therefore characterises the print anisotropy. For instance, a morphologically isotropic print will have $k_y/k_x = 1$, while for long features in the printing direction $k_y/k_x < 1$.

2.4. Electrical characterisation

Due to the typical size of the morphological features and their varying anisotropic nature, four-point probe testing was not suitable as the probe size and inter-probe distance were the same order of size as the morphological features of interest. As such, a custom probe was fabricated consisting of two copper strips 16 mm long and 450 µm thick fixed 16 mm apart as pictured

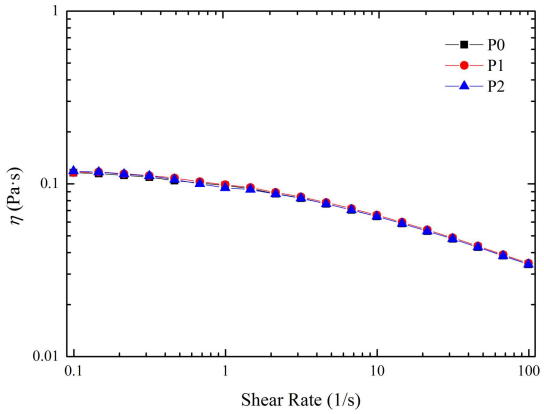

Figure 4: Apparent viscosity η with shear rate for all inks.

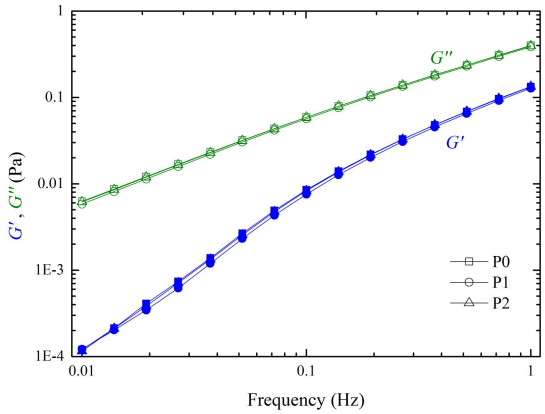

Figure 5: Typical G' (filled symbols) and G'' (unfilled symbols) with frequency for all inks.

in Figure 3. The resistance of each print square was measured both perpendicular and parallel to the printing direction and a load of 0.18 N was applied to the contacts to ensure consistent probe-sample contact. The resistance between the copper strips was recorded as R_x and R_y (perpendicular and parallel to the printing direction, respectively) and the ratio R_y/R_x was calculated as a measure of electrical anisotropy. This technique was able to provide a repeatable measure of the prints' electrical performance and a direct directional comparison, despite the presence of exaggerated non-uniformity. Characterisation of print samples was carried out in a temperature-controlled room (20 ± 1 °C/~40% RH).

In order to confirm that each ink displayed identical electrical properties, an RK Print Coat Instruments K Control Coater was used to bar coat 250 µm PET with a nominally 12 µm thick layer of ink (this being comparable to the print thickness achieved from the anilox volume employed herein [38]). After drying, the samples were cut into 18.75x18.75 mm squares and their sheet resistance was measured using a four-point probe [39]. Optical density measurements of these coated samples were performed using a Spectrolino by Gretag Macbeth.

3. Results and Discussion

3.1. Ink characterisation

The apparent viscosity, η, of each ink as a function of shear rate is shown in Figure 4. All inks show mild shear thinning properties with η decreasing from approximately 0.1 Pa·s to about 0.03 Pa·s over three orders of shear rate. This is qualitatively typical of aqueous PEDOT:PSS solutions [40]. Notably, all three inks exhibit near identical shear viscosity profiles. Elastic and viscous moduli, G' and G'' respectively, are shown as a function of frequency in Figure 5 for all inks. The similarity of G'' for each formulation is consistent with the viscosity measurements of Figure 4. Interestingly, G' is also similar between inks, in contrast to measurements of PVA/PAM blends that show increasing G' with PAM content [21]. Furthermore, G' measurements for the present inks are an order of magnitude higher than those seen by Morgan et al. [21], suggesting that PEDOT:PSS, not PVA or PAM, is the main contributor to the shear elasticity.

Midfilament diameter profiles from extensional rheometry measurements are shown in Figure 6. Breakup times increase considerably with PAM content and the PAM-containing inks both show exponential decay which is characteristic of elastic behaviour [29]. After an initial retardation, likely due to gravitational drainage, filament breakup of ink P0 becomes more linear, with fitting of equation 2 revealing an extensional viscosity $\eta_E = 0.18 \pm 0.01$ Pa·s. This is not inconsistent with the Trouton ratio $\eta_E = 3\eta$ for Newtonian fluids [41], considering the viscosity range shown in Figure 4, suggesting inelastic behaviour in extension. The extensional relaxation times of inks P1 and P2, determined by fitting equation 3 to the elasto-capillary regime of filament breakup, are shown in Table 2 and increase considerably with PAM content. Furthermore, Figure 7 shows filaments observed during CaBER for inks P0 and P2. The curvature of that formed from ink P0 is consistent with Newtonian behaviour and the slender, cylindrical nature of P2 is characteristic of extensionally elastic fluids. [32] While the viscous and elastic behaviour in shear is very similar for all three inks, the

Table 2: Properties of the formulated inks: surface tension (σ), shear viscosity (η) at 1 s^{-1}, elastic modulus (G') at 1 Hz and extensional relaxation time (λ_E) in addition to sheet resistance (R_s) and optical density (OD) of bar coated samples.

Ink	σ (mN/m)	η (mPa·s)	G' (Pa)	λ_E (ms)	R_s (kΩ/□)	OD
P0	42.8 ± 1.5	99.0 ± 1.7	0.133 ± 0.002	-	0.57 ± 0.03	0.340 ± 0.004
P1	43.4 ± 2.5	98.6 ± 1.9	0.128 ± 0.001	78 ± 4	0.59 ± 0.02	0.323 ± 0.007
P2	42.9 ± 2.0	97.3 ± 2.2	0.138 ± 0.007	133 ± 4	0.64 ± 0.02	0.312 ± 0.003

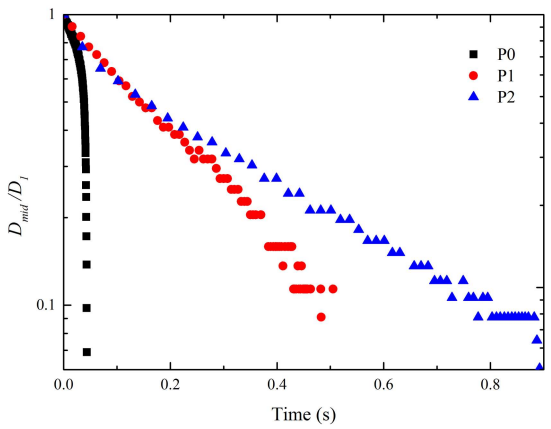

Figure 6: Typical normalised CaBER filament diameter with time for each ink.

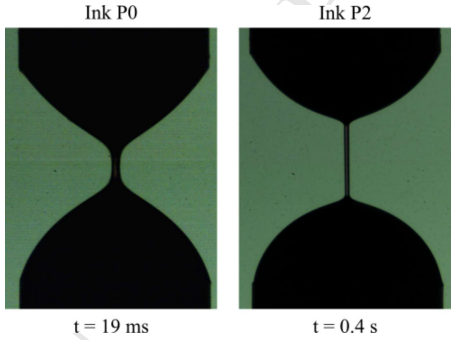

Figure 7: Images of filamentation in CaBER for inks P0 and P2 at similar $D_{mid}(t)$.

elasticity under extensional flow conditions varies substantially. This novel class of fluids therefore allows for the isolation and analysis of effects related to extensional flows in complex processes.

3.2. *Print uniformity analysis*

Print samples for the three inks printed at three different velocities are shown in Figure 8 with non-uniformity akin to viscous fingering being displayed in all prints. The extensionally inelastic ink, P0 exhibits a near-continuous striping in the printing direction at 0.2 and 0.6 m/s. This characteristic is disrupted with increased λ_E, possibly as a consequence of increased wandering and merging of ribs. This is consistent with the convergence of the fingers in the printing direction. An apparent increase in the prevalence of darker dots as λ_E is increased suggests filamentation is also occurring, which has been previously observed in elastic inks due to the rupture of advanced ribs [22]. Increasing v appears to result in a more branched morphology, with further disruption of the longer, striped features. This behaviour was quantified by calculating the average wavenumbers k_x and k_y and the ratio between them k_y/k_x which is plotted in Figure 9(a) as a function of λ_E, with λ_E of ink P0 taken to be zero. As k_y/k_x is always less than 1, $k_x > k_y$ confirming the finger-like features are oriented in the printing direction. The ratio is seen to increase with increasing λ_E and v signifying a more isotropic morphology. These phenomena can be confirmed by visual inspection of the prints and may be attributed to a significant increase in surface undulation in the y-direction as k_x decreased only slightly with v and λ_E. Error bars on Figure 9(a) represent standard deviations of different print samples which are considerable for P0 at the highest velocity. However, as the extensional elasticity is increased the variation between prints at this velocity is reduced, suggesting a more repeatable print outcome was achieved.

The aforementioned Deborah number De may be employed to consolidate the variables v and λ_E and is used to plot k_y/k_x in Figure 9(b) for all non-zero values of De (inks P1 and P2). The wavenumber ratio, and therefore print isotropy, increases with De. Furthermore, the data collapse to a single linear line, highlighting the strong relation between ink extensional elasticity, print velocity and print isotropy. This is of particular interest with regards to the tailoring of ink rheology for desired printed patterns.

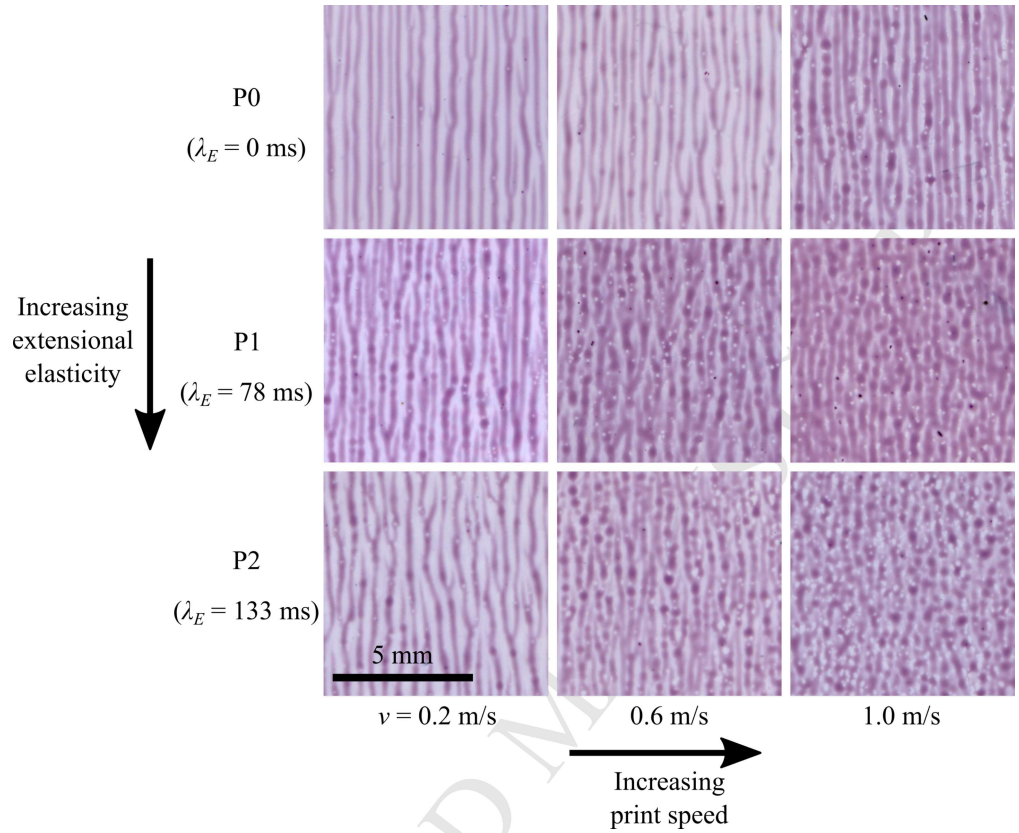

Figure 8: Print samples of the three inks at each printing velocity with brightness adjusted for visual representation.

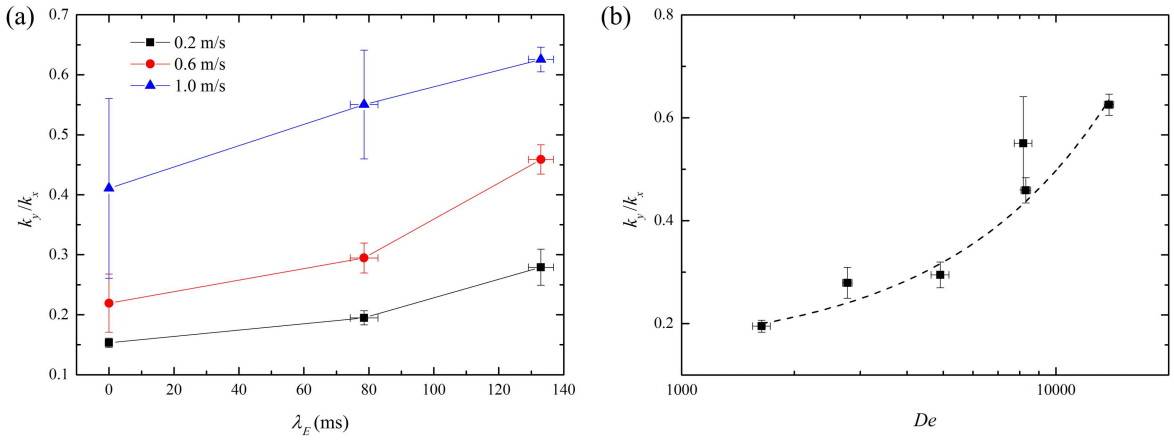

Figure 9: Morphological wavenumber ratio k_y/k_x plotted with (a) extensional relaxation time λ_E and (b) Deborah number De.

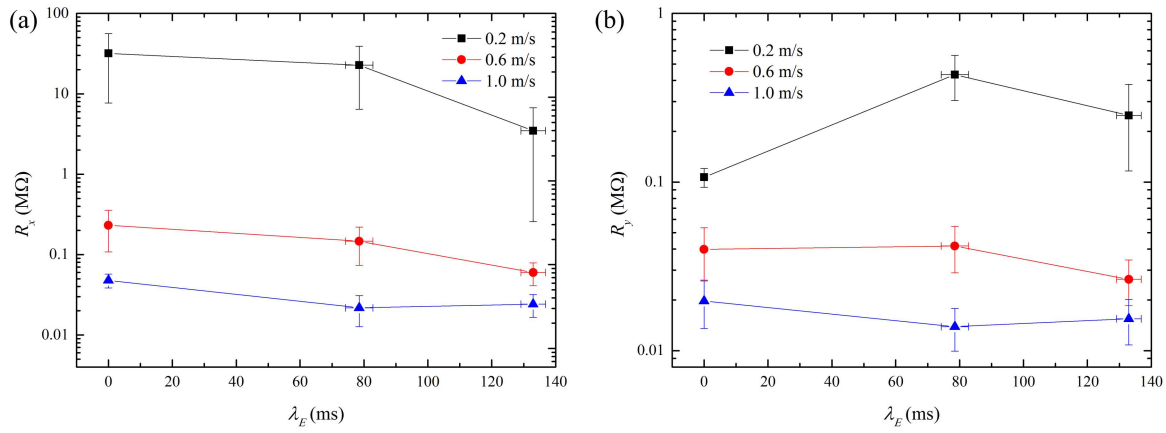

Figure 10: Resistance measured (a) in the x-direction and (b) in the y-direction with extensional relaxation time λ_E.

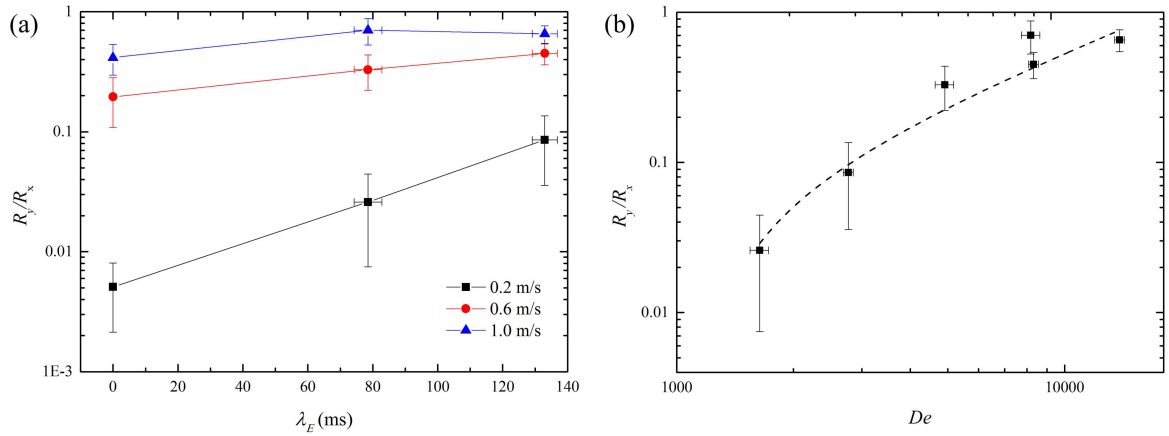

Figure 11: Resistance ratio R_y/R_x with (a) extensional relaxation time λ_E and (b) Deborah number De.

3.3. Electrical characterisation

The sheet resistance R_s of the bar-coated samples of each ink is displayed in Table 2. All three inks have similar sheet resistances although a slight increase is seen with PAM content. This is thought to be due to a minor difference in coated layer thickness rather than detrimental effects of PAM addition, a notion supported by optical density measurements given in Table 2 that show a decrease with PAM content.

Apparent print resistance, measured in the x- and y-directions is displayed in Figure 10(a) and (b) respectively as a function of λ_E. Notably, contact resistance between the probe and print surface, determined by transfer line measurement, was found to be $\sim$ 2 kΩ - an order of magnitude smaller than the lowest sample values.

Print velocity appears to have a significant influence on print resistance in each direction, with increasing v resulting in a decrease of both R_x and R_y. This is possibly due to the shear thinning nature of the inks facilitating transfer at higher speeds and enabling the deposition of a thicker layer. A general reduction in R_x occurs with λ_E, shown in Figure 10(a), which coincides with the apparent increase in branching in the x-direction. This is particularly apparent at 0.2 m/s, where R_x is reduced by an order of magnitude as λ_E is increased from from 0 to 133 ms. Along the prints, as seen in Figure 10(b), λ_E has a less conclusive impact except at 0.2 m/s, where R_y increases by a factor of four from inks P0 (λ_E = 0 ms) to P1 (λ_E = 78 ms). It is possible that disruption

of the continuous morphological features resulted in a more electrically resistive path in the y-direction.

The ratio R_y/R_x provides a comparison of the electrical performance in each direction and is shown as a function of λ_E in Figure 11(a). As both λ_E and v are increased R_y/R_x increases closer to unity suggesting more isotropic electrical properties. In the most extreme case of electrical anisotropy, the extensionally inelastic P0 at the lowest print velocity, the resistance across the print R_x is about 300 times that of the resistance along it, R_y. This print also has the lowest k_y/k_x and is therefore the most morphologically anisotropic. R_y/R_x is plotted with the non-zero Deborah numbers in Figure 11(b) where the data collapse to a linear line suggesting rheological correlation with electrical print performance. This is a significant result regarding the optimisation of device functionality through ink rheology and even indicates that printing instabilities may be used as a low-cost, scalable means of obtaining anisotropic conductive layers.

3.4. Morhpological vs electrical properties

The previously defined ratios k_y/k_x and R_y/R_x provide measures of the morphological and electrical anisotropy of the prints and are plotted together in Figure 12. They exhibit a generally linear relationship with a gradient of approximately 1, showing a clear relation between the orientation of printed patterns and directional electrical performance. As the wavenumber ratio k_y/k_x approaches unity - signifying a more isotropic morphology - so too does the electrical resistance ratio R_y/R_x. This suggests the orientation of printed features, in this case non-uniformity caused by surface instabilities, has a direct link to the resistance of a print in a given direction. Ink rheology and process parameters have therefore been used to control the nature of printed patterns which have in turn dictated the prints' directional electrical performance. This presents a new way of obtaining specific printed patterns and control of print functionality.

4. Conclusions

Conductive model rheological inks were formulated to assess the influence of ink rheology on functional print performance. These inks behaved similarly in shear flow but were markedly different in extension, displaying varying degrees of extensional elasticity. When flexographically printed, viscous fingering oriented in the printing direction was observed on all prints. Concurrently, prints were found to be more electrically conductive in the direction of the finger-like features. As

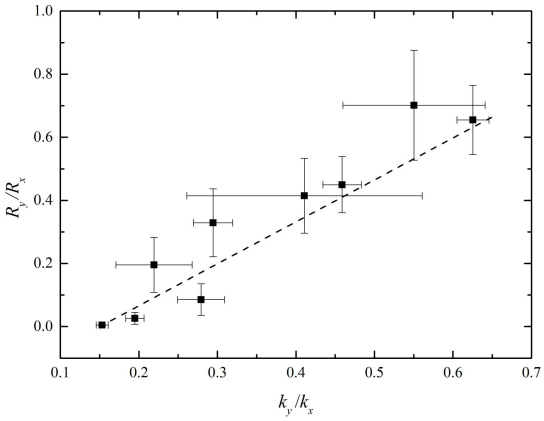

Figure 12: Resistance ratio R_y/R_x against morphological wavenumber ratio k_y/k_x.

ink extensional elasticity and print velocity increased these features became less continuous and the prints became morphologically more isotropic. This was further reflected in the electrical behaviour, with resistance measured along and across the prints becoming more alike. While control was obtained over the nature of the printed patterns, the inhomogeneities were not eliminated altogether. Future work to achieve smooth, uniform layers may hence consider probing wider ranges of the capillary and Deborah numbers or additional treatments of the substrate, plate and prints.

Ink rheology has therefore been shown to influence not only the morphological nature of flexographic prints, but also their functional performance. This emphasises the importance of rheology in functional printing and advances the prospect of tailoring ink rheology for desired print properties.

Acknowledgements

This work was supported by the EPSRC grant number EP/M008827/1.

References

[1] H. Kipphan, Handbook of Print Media: Technologies and Production Methods, Springer, 2001.

[2] D. Deganello, J. A. Cherry, D. T. Gethin, T. C. Claypole, Impact of metered ink volume on reel-to-reel flexographic printed conductive networks for enhanced thin film conductivity, Thin Solid Films 520 (2010) 2233–2237.

[3] H. Yan, Z. Chen, Y. Zheng, C. Newman, J. R. Quinn, F. Dötz, M. Kastler, A. Facchetti, A high-mobility electron-transporting polymer for printed transistors, Nature 457 (2009) 679–687.

[4] J. Benson, C. M. Fung, J. S. Lloyd, D. Deganello, N. Smith, K. S. Teng, Direct patterning of gold nanoparticles using flexographic printing for biosensing applications, Nanoscale Research Letters 10 (2015) 127.

[5] S. Alem, N. Graddage, J. Lu, T. Kololuoma, R. Movileanu, Y. Tao, Flexographic printing of polycarbazole-based inverted solar cells, Organic Electronics 52 (2018) 146–152.

[6] J. Baker, D. Deganello, D. Gethin, T. Watson, Flexographic printing of graphene nanoplatelet ink to replace platinum as counter electrode catalyst in flexible dye sensitised solar cell, Materials Research Innovations 18 (2) (2014) 86–90.

[7] H. M. Sauer, N. Bornemann, E. Dörsam, Viscous fingering in functional flexo printing: an inevitable bug?, Proceedings of the Large-area, Organic and Printed Electronics Convention (LOPE-C).

[8] H. M. Sauer, D. Daume, E. Dörsam, Lubrication theory of ink hydrodynamics in the flexographic printing nip, Journal of Print and Media Technology 4 (3) (2015) 163–172.

[9] M. Hösel, F. C. Krebs, Large-scale roll-to-roll photonic sintering of flexo printed silver nanoparticle electrodes, Journal of Materials Chemistry 22 (31) (2012) 15683–15688.

[10] Z. Wang, R. Winslow, D. Madan, P. K. Wright, J. W. Evans, M. Keif, X. Rong, Development of MnO2 cathode inks for flexographically printed rechargeable zinc-based battery, Journal of Power Sources 268 (2014) 246–254.

[11] P. Saffman, G. Taylor, The penetration of a fluid into a porous medium or Hele-Shaw cell containing a more viscous liquid, Proc. R. Soc. A 245 (1958) 312–329.

[12] C. Voß, Analytische modellierung, experimentelle untersuchungen und dreidimensionale gitter-boltzmann-simulation der quasistatischen und instabilen farbspaltung, Ph.D. thesis, Bergische Universitt Gesamthochschule Wuppertal (2002).

[13] M. Reiner, The deborah number, Physics Today 17 (1964) 62.

[14] R. Bird, W. Stewart, E. Lightfoot, D. Klingenberg, Introductory Transport Phenomena, John Wiley and Sons Ltd, 2015.

[15] H. A. Lécuyer, J. P. Mmbaga, R. E. Hayes, F. H. Bertrand, P. A. Tanguy, Modelling of forward roll coating flows with a deformable roll: Application to non-Newtonian industrial coating formulations, Computers and Chemical Engineering 33 (9) (2009) 1427–1437.

[16] J. R. A. Pearson, The instability of uniform viscous flow under rollers and spreaders, Journal of Fluid Mechanics 7 (4) (1960) 481–500.

[17] R. H. Fernando, J. E. Glass, Dynamic uniaxial extensional viscosity (DUEV) effects in roll application II: Polymer blend studies, J. Rheol. 32 (2) (1988) 199–213.

[18] G. A. Zevallos, M. S. Carvalho, M. Pasquali, Forward roll coating flows of viscoelastic liquids, J. Non-Newtonian Fluid Mech. 130 (2005) 96–109.

[19] M. S. Owens, M. Vinjamur, L. E. Scriven, C. W. Macosko, Misting of Newtonian Liquids in Forward Roll Coating, Industrial & Engineering Chemistry Research 50 (6) (2011) 3212–3219.

[20] E. Pitts, J. Greiller, The flow of thin liquid films between rollers, Journal of Fluid Mechanics 11 (1) (1961) 33–50.

[21] M. L. Morgan, A. Holder, D. J. Curtis, D. Deganello, Formulation, characterisation and flexographic printing of novel Boger fluids to assess the effects of ink elasticity on print uniformity, Rheologica Acta 57 (2) (2018) 105–112.

[22] M. S. Owens, M. Vinjamur, L. Scriven, C. Macosko, Misting of non-Newtonian liquids in forward roll coating, Journal of Non-Newtonian Fluid Mechanics 166 (19-20) (2011) 1123–1128.

[23] O. Carr, G. Gozzi, L. F. Santos, R. M. Faria, D. L. Chinaglia, Analysis of the electrical and optical properties of PEDOT:PSS/PVA blends for low-cost and high-performance organic electronic and optoelectronic devices, Translational Materials Research 2 (1) (2015) 015002.

[24] C. H. Chen, A. Torrents, L. Kulinsky, R. D. Nelson, M. J. Madou, L. Valdevit, J. C. Larue, Mechanical characterizations of cast Poly(3,4-ethylenedioxythiophene): Poly(styrenesulfonate)/Polyvinyl Alcohol thin films, Synthetic Metals 161 (21-22) (2011) 2259–2267.

[25] F. A. Aouada, M. R. Guilherme, G. M. Campese, E. M. Girotto, A. F. Rubira, E. C. Muniz, Electrochemical and mechanical properties of hydrogels based on conductive poly(3,4-ethylene dioxythiophene)/poly(styrenesulfonate) and PAAm, Polymer Testing 25 (2) (2006) 158–165.

[26] S. Khandavalli, J. P. Rothstein, Ink transfer of non-Newtonian fluids from an idealized gravure cell: The effect of shear and extensional deformation, Journal of Non-Newtonian Fluid Mechanics 243 (2017) 16–26.

[27] B. E. Owolabi, D. J. C. Dennis, R. J. Poole, Turbulent drag reduction by polymer additives in parallel-shear flows, Journal of Fluid Mechanics 827 (2017) R4.

[28] J. H. Yu, S. V. Fridrikh, G. C. Rutledge, The role of elasticity in the formation of electrospun fibers, Polymer 47 (2006) 4789–4797.

[29] G. H. Mckinley, Visco-elasto-capillary thinning and break-up of complex fluids, Annual Rheology Reviews 3 (2005) 1–49.

[30] T. R. Tuladhar, M. R. Mackley, Filament stretching rheometry and break-up behaviour of low viscosity polymer solutions and inkjet fluids, J. Non-Newtonian Fluid Mech. 148 (2008) 97–108.

[31] D. T. Papageorgiou, On the breakup of viscous liquid threads, Physics of Fluids 7 (1995) 1529–1544.

[32] G. H. McKinley, A. Tripathi, How to extract the Newtonian viscosity from capillary breakup measurements in a filament rheometer, J. Rheol. 44 (2000) 653–670.

[33] A. V. Bazilevsky, V. M. Entov, A. N. Rozhkov, Liquid filament microrheometer and some of its applications, Proceedings of Third European Rheology Conference and Golden Jubilee Meeting of the British Society of Rheology (1990) 41–43.

[34] R. M. Bidwell, J. L. Duran, G. L. Hubbard, Tables for the determinaton of the surface tensions of liquid metals by the pendant drop method, University of California Los Alamos Scientific Laboratory (1964) 1–11.

[35] C. A. Schneider, W. S. Rasband, K. W. Eliceiri, NIH Image to ImageJ : 25 years of image analysis, Nature Methods 9 (7) (2012) 671–675.

[36] Wolfram Research, Inc., Mathematica Version 10.1, 2015.

[37] N. Otsu, A threshold selection method from gray-level histograms, IEEE Transactions on Systems Man Cybernet SMC-9 (1) (1979) 62–66.

[38] J. A. Cherry, Ink release characteristics of anilox rolls, Ph.D. thesis, University of Wales Swansea (2007).

[39] F. M. Smits, Measurement of sheet resistivities with the four-point probe, Bell System Technical Journal 37 (3) (1958) 711–718.

[40] R. P. Raja Ashok, M. S. Thomas, S. Varughese, Multi-region to single region shear thinning transitions in drying PEDOT:PSS dispersions: contributions from charge density fluctuations, Soft Matter 11 (43) (2015) 8441–8451.

[41] H. A. Barnes, J. F. Hutton, K. Walters, An Introduction to Rheology, Elsevier Science Publishers B.V., 1989.

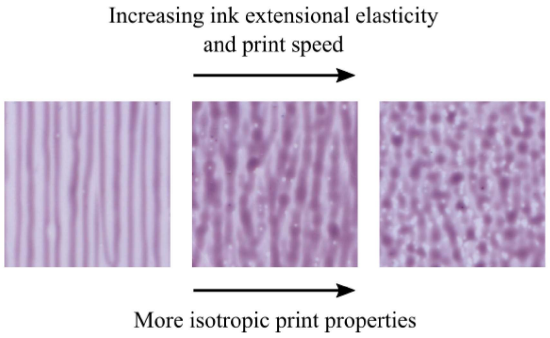

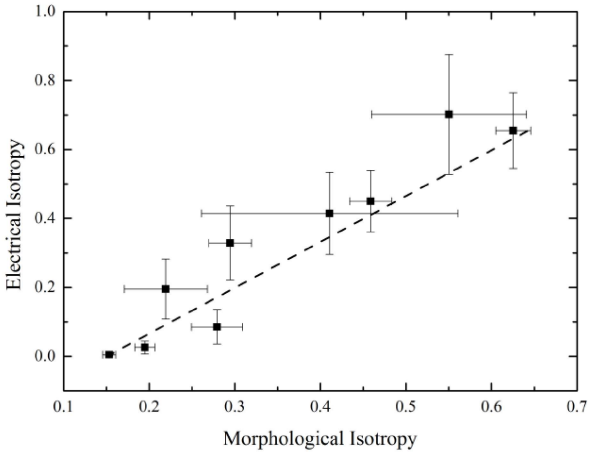

Highlights

- Ink rheology was used to control flexographic print properties.
- Extensional elasticity of PEDOT:PSS inks was manipulated with polyacrylamide.
- Increasing ink extensional elasticity and print velocity enhanced print isotropy.
- Strong correlation was found between morphological and electrical print anisotropy.